D 4   Inelastic scattering: Lattice, magnetic and electronic excitations.

Jörg Voigt

Jülich Centre for Neutron Science

Forschungszentrum Jülich GmbH

Contents

1   What do we want to measure?

In a former lecture, lattice vibrations (phonons) and magnetic excitations (magnons) in solids have been derived theoretically. In the present lecture I will show, how such collective excitations can be measured.

The thermal properties of a material depend on how the constituents move on a microscopical scale. How the atoms/molecules move determines e.g. how heat is transported, what happens at phase transition and how lattice, spin, electronic etc. degrees of freedom interact... The present lecture emphasizes the measurements of lattice and spin excitations. Electronic excitations are only covered as they are involved in the resonant inelastic x-ray scattering process, which is an emergent technique to study magnetic excitations with x-ray.

Phonons and magnons are characterized by their dispersion relations, i.e. $\hbar\omega = f(\mathbf{q})$. Here $\hbar\omega$ denotes the Eigenvalue of the Hamiltonian and $\hbar\mathbf{q}$ the momentum of the excitation. Hence the probes we use for spectroscopy must exchange energy and momentum with the system under study. Typical excitation energies range from a few meV up to several 100 meV. The momentum is governed by the interatomic distances in the sample, which are on the nm scale. Probes that carry the respective momentum are e.g. photons with an energy of several keV, neutrons in the thermal energy range, electrons or α particles. So if the probes are scattered by the sample, the momentum transfer tells us, where the atoms in the material reside. The energy transfer tells us about the bonding of an atom. If the experiment resolves both momentum and energy transfer, we get the detailed information about how the atoms can move in a crystal, i.e. the information about the dispersion relation, which can then be compared to theoretical models describing the sample under study. Light scattering methods, e.g Raman or Brillouin scattering, are employed to investigate elementary excitations in the Brillouin zone centre. Electrons and ions can be used as probes for near surface properties, which may coincide with the behavior in the bulk of a material or may exhibit additional interesting features due to the loss of translational symmetry. This lecture covers inelastic scattering of neutrons and x-ray photons as bulk probes, which penetrate deeply into the sample and provide access to the dispersion relation across the whole Brillouin zone.

1.1   A 'simple' dispersion

Fig. 1 shows a 'simple' dispersion relation, as it has been derived in the lecture of Karin Schmalzl (B4). The dispersion relation for lattice excitations describes, how the displacements of the atoms from their equilibrium position change the energy of the crystal. As the atoms are bonded inside the crystal, the displacement of a single atom forces the other atoms to be displaced, too. The symmetry and the bonding details will determine how the displacement pattern will then look like. In the quantized picture we call such an excitation of the whole lattice a phonon.
Due to the translational symmetry, the phonon can be labeled by its momentum, which is proportional to the reciprocal lattice vector that describes the displacement pattern. All possible phonons can be expressed by reciprocal lattice vectors in the first Brillouin zone grace to the discrete nature and the translational symmetry of the real lattice. From the experimental point of view one may therefore choose a certain reciprocal lattice point and study the Brillouin zone starting from this centre called Γ point.
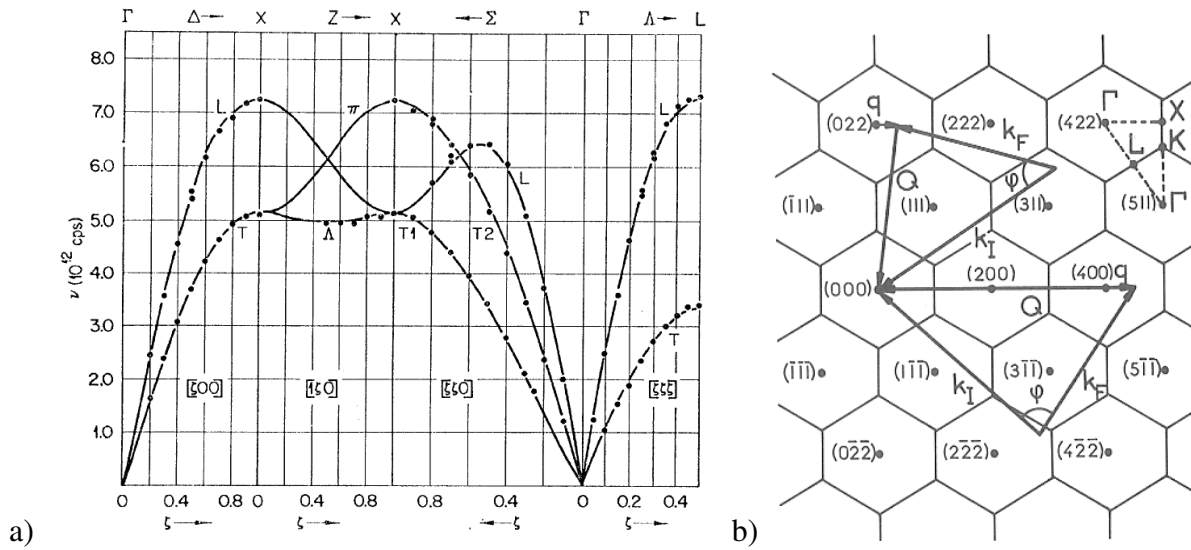
Fig. 1: *a) Dispersion relation for bcc copper along different main symmetry directions. b) Scattering plane in reciprocal plane. Indexed dots refer to Bragg points of the fcc Cu. Two scattering triangles spanned by the initial and final wave vector k and k′ are indicated, one for the measurement of transverse modes and one for longitudinal modes. The dashed triangle in the upper right indicates the nomenclature for high symmetry points in the Brillouin zone. Taken from [1]*

Similar dispersion relations exist for the quantized excitations of the spin system. The that case one can only expect a response of the sample, if the probe interacts with the magnetic moments. For neutrons this interaction is comparable to the nuclear interaction, while for x-ray it is only a relativistic correction to the dominant charge scattering. However, resonance effects can acquire sensitivity to magnetic moments via spin-orbit coupling as will be discussed in sec. 4.3. To find out, where the atoms are and how they move in a sample, the probe excites phonons or magnons, respectively. The scattering obeys energy, momentum and angular momentum conservation. Hence we need to measure the momentum, energy and possibly angular momentum transfer onto the probes in an actual scattering experiment. In sec. 2 the relations between probe and the sample momentum and energy will be derived, before I explain in sec. 3, how the measurement is actually done. The details of the interaction between sample and probe will influence the scattered intensity and further characterize the properties of the excitation as detailed in sec. 4.

2 Scattering

2.1 Kinematics

Elastic scattering   It is instructive to start the explanation of energy and momentum transfer with the visualisation of a diffraction experiment (elastic scattering) in reciprocal space. Let us take a look at the reciprocal space of a simple cubic lattice. In Fig. 2 a part of the plane perpendicular to a [100] direction is shown, which exhibits a quadratic arrangement of reciprocal lattice dots. They represent possible Bragg reflections. If the crystal is perfect except for a

a)   b)
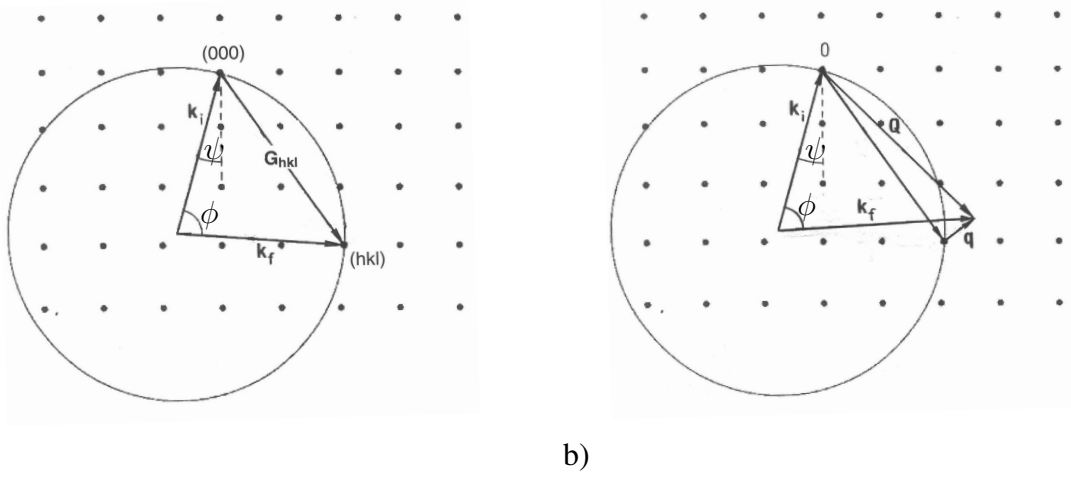
Fig. 2: *a) Reciprocal space and vector representation for elastic scattering: the {100} zone of a simple cubic lattice showing Ewald's construction for Bragg reflection. The number (letters) in brackets denote the Miller indices of the reciprocal lattice vector τ. b) Reciprocal space and vector representation for inelastic scattering: The momentum transferred to the sample is the sum of the reciprocal lattice vector τ and the momentum transfer q to a phonon within the Brillouin zone around τ.*

certain degree of mosaicity (micro crystallites are all aligned within a small deviation η from a given orientation), the elastic scattering is confined to the Bragg dots. For elastic scattering is $|k'| = |k| = k$. The circle with radius k (the Ewald circle, respectively sphere in three dimensions) contains the origin of the reciprocal space and at least one other point of the reciprocal lattice of the crystal. The circle contains all scattering vectors $Q = k' - k$ for a fixed k. The condition

$$Q = \tau = k' - k \tag{1}$$

is nothing more than the familiar Bragg condition expressed in vector notation. The norm of eq. 1 gives

$$|Q| = |\tau| = \frac{2\pi}{d_{hkl}} = 2k \sin \theta = \frac{4\pi}{\lambda} \sin \theta$$

$$\Leftrightarrow n\lambda = 2d_{hkl} sin\theta. \tag{2}$$

In this equation d_{hkl} denotes the interplanar spacing of the lattice planes with Miller indices h, k, l. θ is the glancing angle of reflection from these planes. n can take any integer value. Hence integer fractions of the fundamental wavelength ($n = 1$) satisfy the reflection condition as well. By adjusting the the scattering angle $2\theta = \phi$ between k and k' the norm of Q is controlled. The orientation of Q is set by the sample rotation ψ. Thus, any point in reciprocal space can be reached by an appropriate choice of the incident wave vector k, the scattering angle ϕ and the sample orientation ψ relative to k.

Inelastic scattering   For inelastic scattering, the situation is more complicated. Since energy is transferred between the sample and the neutron, the norm of k and k' is different. In that case,
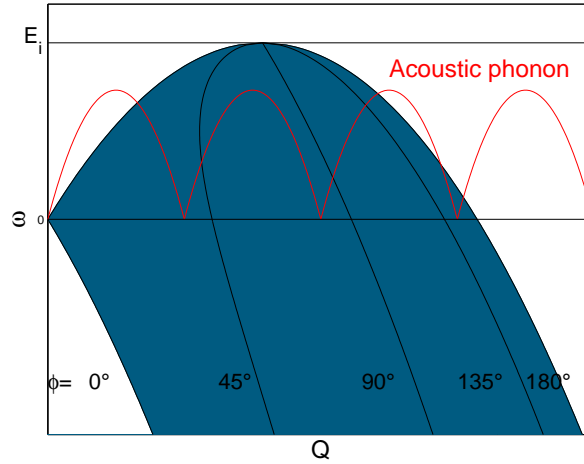
Fig. 3: *Relation between norm of the momentum transfer $\hbar Q$ and $\hbar\omega$ for different values of the scattering angle ϕ for neutron scattering. The blue area encloses the accessible Q, ω space. Black lines indicate the scattering angle Φ. As detectors cannot cover all angles, the region measured is slightly smaller. Positive values of ω correspond to energy loss of the neutron. Acoustic phonon branches in several Brillouin zones are shown as well. Note: For small momentum transfer, a phonon cannot be observed, if the sound velocity within the sample is higher than the neutron velocity (the velocities are given by the slope of the respective curves at $Q = 0$). For x-ray scattering the whole area is accessible, as the photon energy is 4 to 5 orders of magnitude larger than the excitation energy.*

the diagram 2a) has to be modified as shown in Fig. 2b). Writing down momentum and energy conservation gives:

$$
\begin{align}
Q &= k' - k \tag{3}\\
Q^2 &= k^2 + k'^2 - 2kk' \cos\phi \tag{4}\\
\hbar\omega &= E_i - E_f = \frac{\hbar^2}{2m}(k^2 - k'^2)\,\text{(for neutrons)} \tag{5}\\
\hbar\omega &= E_i - E_f = \hbar c(k - k')\,\text{(for x-ray)} \tag{6}
\end{align}
$$

Combining these equations yields the accessible region in the Q, ω space for a given incident energy E_i, which is limited for neutron scattering (see Fig. 3). The highest accessible energy transfer for a given momentum transfer is given by the cases of forward scattering ($\phi = 0$) and exact backscattering ($\phi = 180$), which can not exactly be accessed in an actual instrument.

The transferred energy $\hbar\omega$ depends in a periodic lattice only on the relative momentum $\hbar q$ defined within a Brillouin zone. Therefore the momentum transfer is referred to the nearest reciprocal lattice vector.

$$
Q = \tau + q \tag{7}
$$

as depicted in Fig. 2b). An acoustic phonon branch has been included in Fig. 3 for several Brillouin zones. Note that an excitation at the origin of the reciprocal space can only be measured, if the sound velocity within the material is smaller than the neutron velocity. This limitation is lifted for the case of inelastic x-ray scattering.
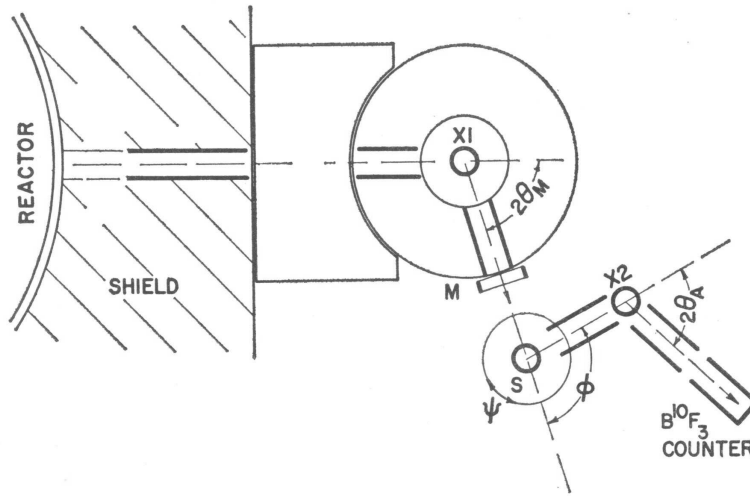
Fig. 4: *Schematic of a triple axis spectrometer. The angle Φ denotes the scattering angle between k, k', the angle ψ gives the orientation of the scattering triangle with respect to the reciprocal lattice of the sample (cp. Fig 1 b). The initial and final wavelength is defined by the scattering angles $2\theta_{M,A}$, respectively.*

3 Methods

3.1 The neutron three axis spectrometer

The most common instrument using Bragg diffraction to prepare and analyse the neutron wavelength is the three axis spectrometer (TAS). In 1994 the Nobel price has been awarded to its inventor Bertram Brockhouse "for pioneering contributions to the development of neutron scattering techniques for studies of condensed matter" and in particular "for the development of neutron spectroscopy".

The particular instrument name stems from the existence of three axes around which important components of the instrument can be rotated (see Fig. 4). In order to select the desired wavelength according to eq. 2, the monochromator as well as the sample table have to be rotated around the first axis in a $\theta - 2\theta$ mode (X1 in Fig. 4). Around the second axis (the sample axis) the analyser/detector unit can be rotated, whereby the sample scattering angle ϕ is selected with respect to the direction of the incoming neutron wave vector k. Around the third axis (X2 in Fig. 4), both the analyser crystal and the detector are rotated in a $\theta - 2\theta$ mode in order to probe the wavelength (energy) of the scattered neutrons. An additional rotation around the sample axis (angle ψ) allows to scan any desired path within the reciprocal space plane spanned by k and k'.

The resolution of a triple axis instrument depends on the relative sense of rotation at the instrument spectrometer axes, as shown in Fig. 5a). The resolution function of a TAS has been derived analytically by Cooper and Nathans [2] and by Popovici [3]. The resolution of the final and initial wave vector depends on the properties of the monochromator and analyzer crystals, respectively:

$$\frac{\Delta\lambda}{\lambda} = \frac{\Delta d_{hkl}}{d_{hkl}} + \cot\theta\Delta\theta \tag{8}$$
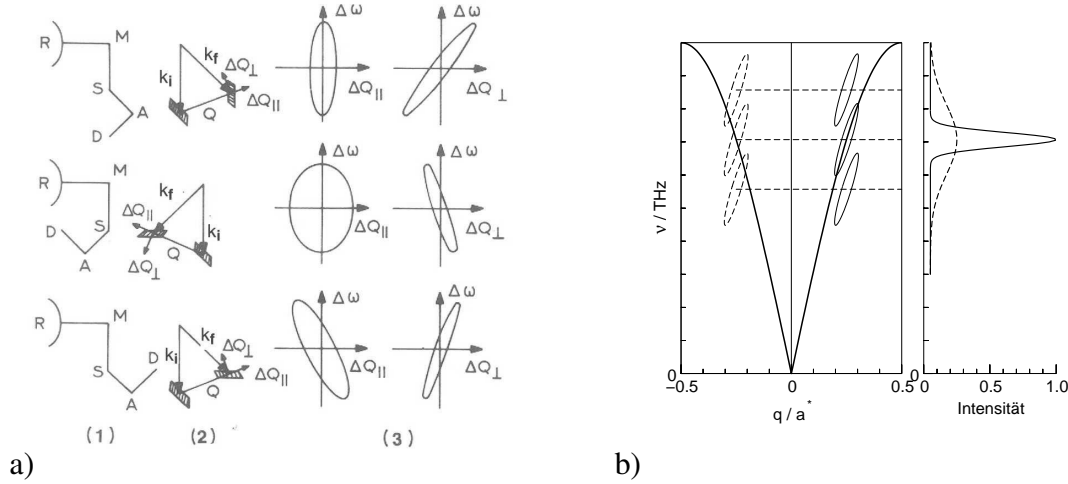
Fig. 5: *a)Resolution volumes of a TAS in different geometries. The hashed areas indicate the deviation of k, k' from their most probable values. From [1]. b) Effect of focusing: If the orientation of the resolution ellipsoid is adopted to the slope of the dispersion, the peak shape of the inelastic signal can be optimized.*

with d_{hkl} denoting the lattice spacing of the (hkl) reflection and θ defined by the scattering angle 2θ. The first contribution to the resolution is mainly determined by the primary extinction length, which describes, how deep the neutron beam penetrates the crystal, when it is in reflection position. Because every mirror plane reflects a part of the incoming intensity, this length is limited to several 10^4 lattice spacings, giving a resolution for a perfect single crystal, which is about 10^{-4}. The second contribution originates from the mosaic spread in a real crystal. It grows for smaller scattering angles 2θ and vanishes, if 2θ approaches 180°. Since the neutron guides, which transport the neutrons from the reactor core to the instrument, determine the divergence that arrives at the monochromator within 1°, a very high resolution would yield only vanishing intensity passing the monochromator. Therefore typical monochromator crystals for neutrons have a rather wide mosaic spread or an artificial variation of the lattice constant. Since the energy of a thermal or cold neutron is on the order of several meV, typical excitations in a solid can be resolved by a 10% resolution of the initial and final energy. The situation is drastically different, if we talk about inelastic x-ray scattering. Typical photon energies are on the order of several keV. Accordingly a resolution power of 10^{-7} is required. Since x-ray beam from a third generation synchrotron is extremely bright, one can effort to minimize every contribution to the resolution and realize an intense beam, that allows the measurement of an inelastic signal.

By an appropriate choice of the scattering geometry, the resolution ellipsoid can be oriented nearly parallel to the dispersion. In that case the folding of the scattering function with the resolution function will be as narrow as possible (cp. Fig 5b)).

3.2   Multiplexing TAS

As explained in the last section three axis spectrometers can be tuned with optimized resolution to any position inside the scattering parabola. To survey the reciprocal space it is then necessary to scan along lines. This can be very time consuming, especially when the signals are weak and every point must be measured for a long time. To improve the mapping capabilities different

multiplexing schemes have been developed [4, 5, 6, 7]. They all have in common that not a single k′ is analyzed but that many analyzer crystals are arranged around the sample to record not a point but a line in reciprocal space. The multiplexing setups are addons to a conventional TAS. They are not as flexible, but they provide the possibility to cover large areas in reciprocal space. Special regions of interest may then be focused by conventional TAS with optimized setting of the resolution conditions with respect to the scientific question.

3.3   Inelastic x-ray scattering

While inelastic neutron scattering is the traditional method to study coherent excitations in matter, there exist several applications that are limited by the neutrons flux of todays neutron sources. Fig. 6a shows an example of IXS from thin films. The high brightness of the synchrotron source provides enough photons to be scattered by the phonons of the thin films. Furthermore the higher absorption of the photons prevents the scattering from the substrate, which causes a strong inelastic signal in the case of the deeper penetrating neutrons. Fig. 6b is an example of high energy phonons, which can easily be accessed by x-ray scattering. If one wants to study such high energies with neutrons either a hot moderator (e.g. Graphite at 2000 K) or a short pulse spallation source with a large number of undermoderated neutrons is required.

Measurements of lattice and excitations with energies $\hbar\omega = 1 - 1000$ meV with photons of energy $E_i = 10 - 50$ keV requires a relative energy resolution better than 10^{-6}. This can be achieved using backscattering from perfect crystals. The setup of the inelastic x-ray scattering beamline ID28 at the ESRF is shown in Fig. 7.
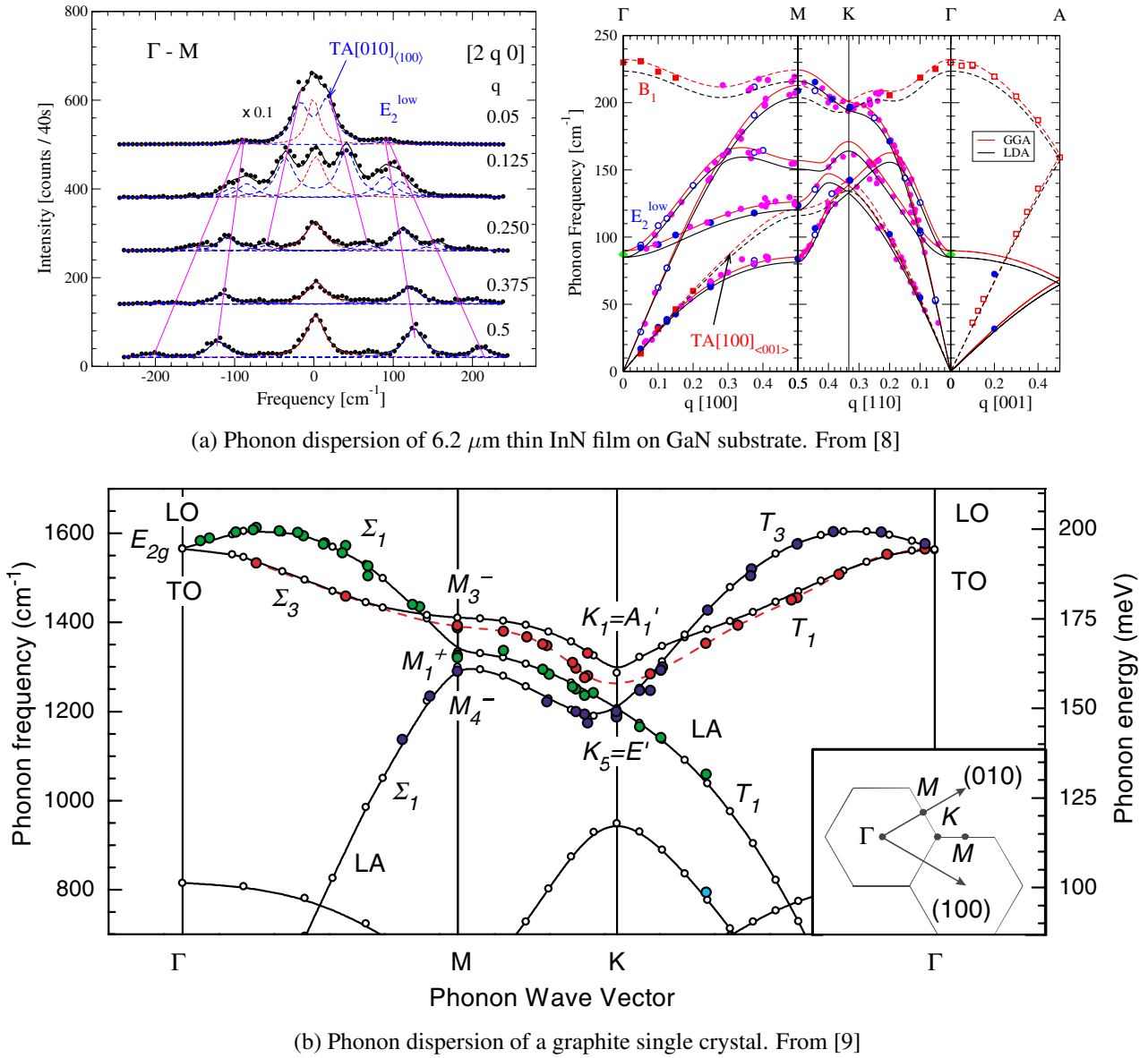After premonochromatization, the initial energy is defined by a flat backscattering monochromator. The penetration of a x-ray beam in a non-absorbing perfect crystal generally referred to as primary extinction length depends on the reflectivity of the single lattice plane of the considered reflection. The higher is the reflectivity, the smaller is the penetration. Going to reflections with large Miller indices increases the resolving power: this is a direct consequence of the reduced form factor for large $|Q|$. A (13 13 13) reflection from a perfect Silicon crystal reaches $\Delta E/E = 10^{-8}$. This resolution has to be matched by the second term in eq. (8) $\cot\theta\Delta\theta$. Taking into account the angular divergence delivered from a third generation synchrotron source ($\Delta\theta \approx 10\mu$Rad) $\cot\theta$ should be smaller than 10^{-4} ($\theta \approx 89.98°$).
After further optical components, the photons are scattered from the sample. The energy resolution of the analyzer should be the same as the monochromator. However, the angular acceptance is defined by the desired Q resolution, which is relaxed as compared to the energy resolution. Typical values for ΔQ range from 0.2 to 0.5 nm^{-1}. This corresponds to an angular acceptance for the analyzer of about 10 mrad. The angular acceptance is obtained by the use of a focusing system. To preserve crystal perfection properties small flat perfect crystals are layed on spherical surface. The curvature is defined by a 1:1 pseudo *Rowland* geometry with aberrations kept such that the energy resolution is not degraded.
The backscattering conditions requires an alternative way to scan the energy transfer. Since the angle is fixed, one has to vary the lattice constant according to the Bragg eq. 2. The energy transfer is determined by the relative temperature between monochromator and analyzer. Considering $\Delta d/d = \alpha\Delta T$, with $\alpha = 2.56 \cdot 10^{-6}$K^{-1}, the temperature has to be controlled with a precision of 0.5 mK to obtain an energy step of about 1 tenth of the energy resolution. The overall resolution of the spectrometer at ID28 is shown in Fig. 8.
   To overcome the constraints set by the backscattering geometry alternative high resolution

(a) Phonon dispersion of 6.2 μm thin InN film on GaN substrate. From [8]

(b) Phonon dispersion of a graphite single crystal. From [9]

Fig. 6: *Examples of phonon studies with inelastic x-ray scattering.*

monochromators have been developed for high resolution synchrotron applications (see [10] and references therein). These monochromators increase the energy resolution by the use of asymmetric Bragg reflections to achieve a higher energy bandwidth than the intrinsic resolution of a single Bragg reflection [11] (see Fig. 9). Such monochromators allow a larger energy range to be scanned. Thermal stability is very important in order not to change the lattice constants. It is furthermore beneficial, when the lattice expansion vanishes at the operation temperature.

3.4   Time-of-flight spectroscopy

In contrast to x-ray photons the neutron is a massive particle and the velocity depends on the energy. Typical velocities for thermal and cold neutrons range from $v_n = 3956 \frac{m}{s}$ for neutrons with $\lambda = 1$ Å to $v_n = 395.6 \frac{m}{s}$ for $\lambda = 10$ Å. The energy is of course proportional to the square
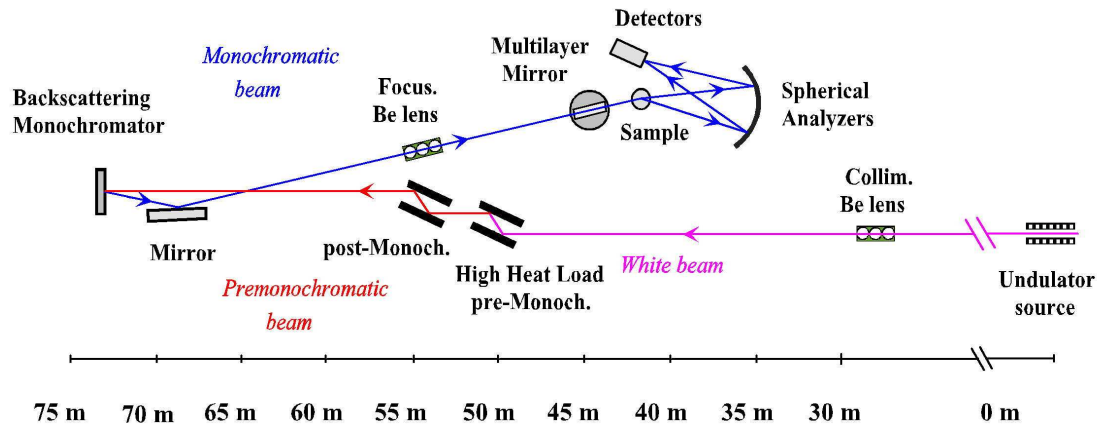
Fig. 7: *Setup of the inelastic scattering beamline ID28 at the ESRF.*
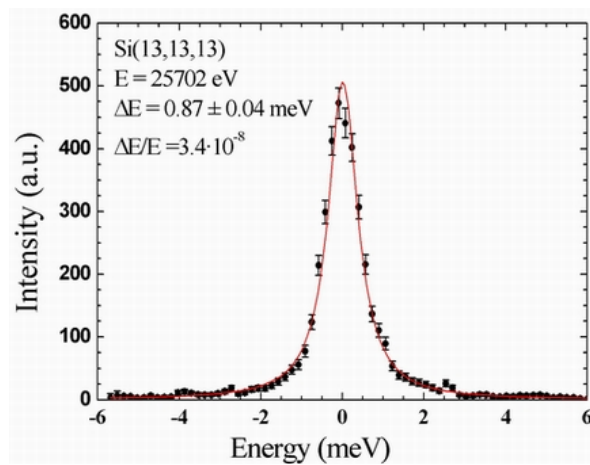
Fig. 8: *Instrumental resolution function of ID28 at the ESRF determined by scattering from a Plexiglas sample at Q=10 nm^{-1} and T=10 K.*
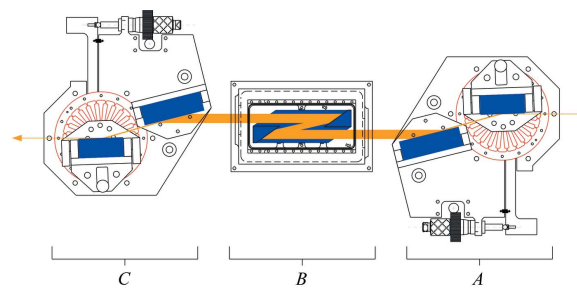
Fig. 9: *Design of a six-reflection cryogenically stabilized high-resolution monochromator. The x-ray beam enters from the right. From [10].*

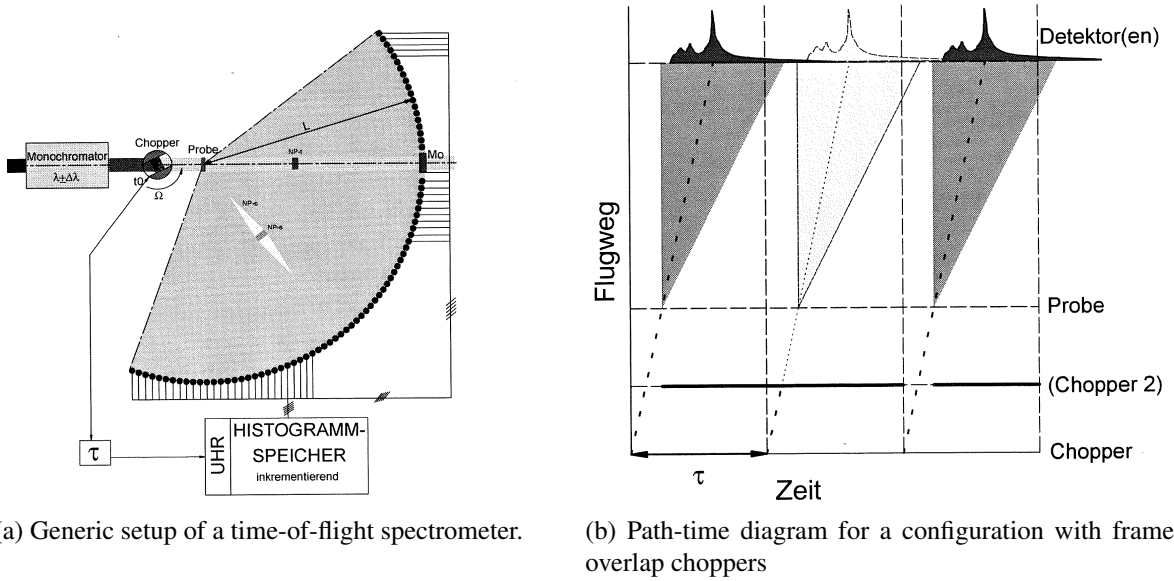|	Neutrons	X-rays
$\lambda[\text{Å}]$	$0.2 - 20$	$0.5 - 40$
$E_i[\text{eV}]$	$0.0818 \cdot \lambda^{-2}$	$12398 \cdot \lambda^{-1}$
$v[\text{m/s}]$	$3956 \cdot \lambda^{-1}$	c
$\Delta\hbar\omega[\text{meV}]$	$10^{-3} - 10$	$50 - 500$
Divergence [rad]	0.01	10^{-6}
Sensitivity		
Phonons	+	+
Magnons	+	(non resonant) -
		(RIXS) +
Electronic excitations	-	+

Table 1: *Comparison Neutron $\leftrightarrow$ x-ray in the wavelength range that is used for spectroscopy.*

of the velocity and inverse of the wavelength λ:

$$E_n = \frac{1}{2}m_n v_n^2 \tag{9}$$

$$= \frac{h^2}{m_n \lambda^2}. \tag{10}$$

Accordingly 1 Å neutrons have an energy of 81.8 meV and 10 Å neutrons have 0.818 meV. This offers an alternative way to measure the energy exchange with the sample: if we define the initial neutron velocity by an appropriate monochromator and define a precise start signal for the neutrons hitting the sample by a chopper, we can analyze the energy exchange to the sample by recording the arrival of the neutrons at the detector in a given distance from the sample and the chopper. In contrast to three axis spectroscopy, the energy can then be determined simultaneously for all scattering angles ϕ. Therefore by covering a large solid angle with detectors, one could measure the complete $\mathbf{Q}, \omega$ space very effectively. However, the decoupling of energy and scattering angle comes for a price: one can use only neutrons in a short burst time $\tau < 20\mu$s and has then to wait until all neutrons arrive at the detector to record the full energy spectrum, before the next pulse can start, see Fig. 10b. So for a time-of-flight instrument at a continuous source, one can use the neutron beam during 1-2% of the time. At short pulse spallation sources, all neutrons are created in a short pulse. For time-of-flight experiments on can therefore us the full peak flux and gain over constant beam sources a factor ≈ 100, even if the time averaged flux is comparable or lower. The intensity scattered into the solid angle $d\Omega$ defined by the desired $\mathbf{Q}$ resolution is still sometimes at the limit of detection. Traditionally time-of-flight spectroscopy is used mainly to study excitations that are not sharply defined in momentum transfer. Then the intensity can be integrated over a larger solid angle. One example is the incoherent one phonon scattering cross section as a measure for the phonon density of states, as it integrates all scattering vectors $\mathbf{Q}$ for a given energy ω. Crystalline electric field excitations that depend mainly on the local environment are another typical application for time-of-flight spectroscopy. With the new Megawatt spallation sources but also with new instruments at reactor sources, as the new TOPAS instrument at the FRM2, the flux limit will be lifted and the full potential of TOF spectroscopy will be available for mapping the excitation landscape in condensed matter research.

(a) Generic setup of a time-of-flight spectrometer.

(b) Path-time diagram for a configuration with frame overlap choppers

Fig. 10: *ToF spectroscopy.*

4 Response

So far we have discussed, how we can tune an neutron or x-ray spectrometer to measure a certain energy and momentum exchange with the sample. Often this is also the major aim of an experiment. Important insight into the dynamics of a system can often be acquired from the knowledge of the dispersion relation. But a scattering experiment can provide more information, which is contained in the scattered intensity.

The inelastic scattering of neutrons and x-ray is usually described in the Born approximation. The information on the dynamics is contained in the scattering function $S(\mathbf{Q}, \omega)$, which is connected to the double differential cross section $\frac{d^2\sigma}{d\Omega\omega}$, the basic quantity in a scattering experiment [12]:

$$\frac{\mathrm{d}^2\sigma}{\mathrm{d}\Omega\mathrm{d}\omega} = A(\mathbf{Q})S(\mathbf{Q}, \omega). \tag{11}$$

The properties of the scattered particle as well as the interaction potential with the sample are included in the factor A.

The scattering function $S(\mathbf{Q}, \omega)$ is the Fourier transform of the pair correlation function, introduced in the lecture of R. Zorn (A5). It depends only on the momentum and the energy transferred to the sample and not on the actual values of k and k′. It contains the information on both the positions and motions of the atoms comprising the sample. Via the dissipation-fluctuation theorem, the scattering function is connected to the dissipative or imaginary part of the dynamical susceptibility [13]:

$$S(\mathbf{Q}, \omega) = \frac{\chi''(\mathbf{Q}, \omega)}{1 - \exp(-\hbar\omega)/(k_B T)} \tag{12}$$

The measured intensity in an actual inelastic scattering experiment is the folding of the resolution function of the instrument with the scattering function in $\mathbf{Q}, \omega$ space:

$$I(\mathbf{Q}, \omega) \propto \iint R((\mathbf{Q}' - \mathbf{Q}), (\omega' - \omega))S(\mathbf{Q}, \omega)d\mathbf{Q}'d\omega' \tag{13}$$

The resolution function R depends on the are a probability distributions $p_{i,f}$ for the initial and final wave vectors:

$$R(\mathbf{Q}, \omega) = \iint p_i(\mathbf{k'_i}) p_f(\mathbf{k'_f}) \delta(\mathbf{Q'} - (\mathbf{k'} - \mathbf{k})) \delta(\omega' - \frac{\hbar}{2m}(\mathbf{k}^2 - \mathbf{k'}^2)) d\mathbf{k'_i} d\mathbf{k'_f} \qquad (14)$$

The normalisation of the resolution function is the product of the volume elements in reciprocal space defined by probability distributions:

$$\iint R((\mathbf{Q'} - \mathbf{Q}), (\omega' - \omega), \mathbf{Q}, \omega) d\mathbf{Q'} d\omega' = V_i(\mathbf{k}) \cdot V_f(\mathbf{k'}) \qquad (15)$$

The intensity one can expect for a given $\mathbf{Q}, \omega$ thus is proportional to this product. These distributions are defined by the collimation on the primary side (before the sample) and the secondary side (between the sample and the detector). Hence it becomes clear that intensity and resolution (defined by the collimation) have to be traded according to the present scientific problem.

4.1   Single phonon scattering

The double differential cross section for coherent single phonon scattering of neutrons contains more information about the system under study than only the dispersion relation, which is contained in the delta function eq. (19) [14]:

$$\left(\frac{d^2\sigma}{d\Omega d\omega} \right)^{\pm}_{coh} = \frac{\mathbf{k'}}{\mathbf{k}} \frac{(2\pi)^3}{v_0} \sum_{\boldsymbol{\tau}} \sum_{j,\mathbf{q}}$$

$$\cdot |\sum_i \frac{b_i}{\sqrt{m_i}} \exp[-W_i(\mathbf{Q}) + i\mathbf{Q} \cdot \boldsymbol{R_i}](\mathbf{Q} \cdot \boldsymbol{e_i^j})|^2 \qquad (16)$$

$$\cdot \omega_j^{-1} \qquad (17)$$

$$\cdot (n(\omega_j(\mathbf{q})) + \frac{1}{2} \pm \frac{1}{2}) \qquad (18)$$

$$\cdot \delta(\omega \mp \omega_j(\mathbf{q})) \delta(\mathbf{Q} \mp \mathbf{q} - \boldsymbol{\tau}) \qquad (19)$$

In the expression for the double differential x-ray scattering cross section, the nuclear scattering length must be replaced by the atomic form factor as long as the photon energy is not close to an absorption edge, but the structure of the cross sections remains the same.

Expression 16 is called the dynamical structure factor, in analogy to the structure factor in elastic scattering. Its strength depends on the nuclear coherent scattering length of the constituting nuclei b_i, which is the mean value of the different scattering length for different isotopes or different nuclear spin. It includes the Debye-Waller factor $\exp[-W], W = \langle \mathbf{Q} \cdot \boldsymbol{u} \rangle^2$, introducing the displacements $\boldsymbol{u}$ of atoms from their equilibrium position.

The intensity is proportional to a factor $|\mathbf{Q} \cdot \boldsymbol{e_i^j}|^2$, with the polarization vector of the phonon mode $\boldsymbol{e_i^j}$. This means, it becomes favorable to measure phonons with large $\mathbf{Q}$. This property provides an opportunity to distinguish between magnetic and lattice excitations. As we will see later, scattering from magnetic excitation becomes less probable for large momentum transfer due to the magnetic form factor. Therefore measurements in different Brillouin zones tell you, whether your signal is of magnetic or nuclear origin.

Due to the scalar product in eq. (16) only if the displacement has a component parallel to the scattering vector $\mathbf{Q}$, the respective mode contributes to the structure factor. In a very pictorial

view you may regard the scattering process as a 'kick' in the direction of the momentum transfer. In the case of phonon creation, the neutrons 'kicks' off the phonon, in the case of annihilation the neutron 'gets kicked' by the phonon. If we compare the different scattering triangles in Fig. 4 b) we see, that in the upper triangle the q is nearly perpendicular to Q. Accordingly we measure at this position a transverse phonon branch, where the displacement is perpendicular to the wave vector. In the lower scattering triangle q and Q are parallel. Hence the neutron can only be scattered by a longitudinal phonon.

The intensity of a phonon mode depends inversely on its energy (eq. 17). Thus high energy phonons become difficult to measure. Expression 18 describes the occupation of a phonon mode. The $+$ sign refers to a phonon creation, the $-$ sign to annihilation.

$$n(\omega_j(\mathbf{q})) = (\exp[\hbar\omega_j(\mathbf{q})/k_b T] - 1)^{-1} \tag{20}$$

is the familiar Bose factor.

As eq. (16) contains the coherent nuclear scattering length that cross section describes the pair correlations in a crystal. Scattering provides also access to purely local dynamics of a scatterer via the incoherent scattering length, which comes from the deviations of the scattering length from different isotopes or different orientation of the neutron spin to the nuclear spin from the mean value. This incoherent scattering is described by the incoherent double differential cross section [14]:

$$\left(\frac{d^2\sigma}{d\Omega d\omega}\right)^{\pm}_{inc} = \frac{k'}{k}\frac{(2\pi)^3}{v_0} \tag{21}$$

$$\sum_i \frac{1}{2M_i}(\overline{b_i^2} - \overline{b_i}^2)\exp(-2W_i(\mathbf{Q})) \tag{22}$$

$$\times \sum_j \frac{|\mathbf{Q}\cdot\mathbf{e}_{ij}|^2}{\omega_j}\cdot\left(n(\omega_j(\mathbf{q})) + \frac{1}{2}\pm\frac{1}{2}\right)\delta(\omega\mp\omega_s) \tag{23}$$

From the incoherent scattering the phonon density of states can be derived, as it integrates over all possible phonon branches for a given energy.

4.2 Magnetic excitations

While in principle x-ray as a electro-magnetic wave could be scattered by the magnetic moments of a sample, the interaction away from the absorption edges is weak for the scattering to be detected by the present instruments. We will later come to the resonant inelastic scattering, which is a higher order scattering process which can be sensitive to magnetic excitations, too.

In contrast neutrons interact with the magnetic moments in the sample with a comparable strength as with the nuclei. Therefore inelastic neutron scattering is still the standard method to study magnetic excitations. The double differential cross sections for single magnon scattering

reads

$$\left(\frac{d^2\sigma}{d\Omega d\omega}\right)^{\pm}_{mag} = \frac{k'}{k}\frac{(2\pi)^3}{v_0} \tag{24}$$

$$\frac{1}{2}S\left(\frac{\gamma r_0}{2}gf(\mathbf{Q})\right)^2 \tag{25}$$

$$\exp\left[-2W(\mathbf{Q})\right] \tag{26}$$

$$(1+\hat{\mathbf{Q}}_z^2) \tag{27}$$

$$\sum_{\tau,\mathbf{q}}\left(n(\omega(\mathbf{q}))+\frac{1}{2}\pm\frac{1}{2}\right) \tag{28}$$

$$\delta(\omega\mp\omega(\mathbf{q}))\delta(\mathbf{Q}\mp\mathbf{q}-\tau). \tag{29}$$

This cross section has several distinct differences from the cross section for single phonon scattering eq. (16). The interaction strength is given by expression (25). It depends on the spin S or more general the total angular momentum J, the gyromagnetic factor of the neutron γ, the classical electron radius r_0, the Lande' factor g and the magnetic form factor $f(\mathbf{Q})$. The form factor reflects the extended distribution of the magnetic moment around the atom, as the outer atomic shells contain the unpaired electrons responsible for the magnetic moment. The expression (27) comes from the selection rule for the magnetic neutron scattering, which states that only the magnetic moment perpendicular to the momentum transfer scatters the neutron, and from the fact that the 1 magnon scattering reduces the magnetic moment in the quantization direction z and increases the x, y components, respectively.

4.3 Resonant Inelastic X-ray Scattering (RIXS)

The cross sections discussed so far provide direct information about the dynamics of the lattice and the spin system and are therefore a solid test for any model describing the spin system. The coupling to the electron system can be investigated only indirectly by studying e.g. the life time of the excitations [15, 16]. In RIXS the opposite way is used: one excites the electron system and investigates, how the excitation couples to the different elementary excitations in the solid [17]. Here we have to distinguish two different processes: direct RIXS and indirect RIXS (Fig. 11).

In the direct process the core electron is excited into an empty valence band state and the core hole is filled by another valence band state. For this process the selection rules must allow both transitions. The direct process is e.g. allowed for the L edges of the transition metals in the soft x-ray regime. They excitations probed by this regime include single magnon excitations [18].

They indirect RIXS process is observed when the core electron is excited into an empty state in the conduction band relatively high above the Fermi energy. The core hole is then screened only weakly and acts as a scattering potential for the valence electrons. Alternatively one could say that the exciton of core hole and conduction band electron scatters off the valence band excitations. After the core hole is filled an electron-hole excitation is left behind in the valence band.

The local nature of the excitation into the intermediate state makes RIXS an element specific technique. It can therefore be used to study the dynamics in the subsystem of a complex material, e.g. the transition metal or the ligand in a transition metal oxide.

In principle RIXS is sensitive to a variety of elementary excitations e.g., plasmons, charge transfer excitations, crystal field excitations, magnons and phonons and more. The sensitivity states
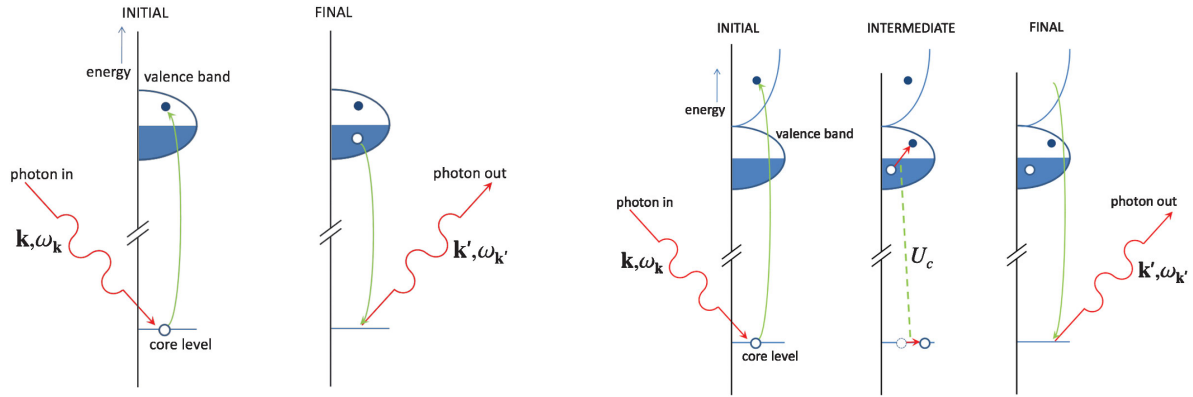
(a) Direct RIXS process: The core electron is excited into an empty valence band state and the core hole is filled by a different valence band state. For both transitions to the core states must be allowed

(b) Indirect RIXS process: The core electron is excited far above the Fermi energy. The core hole potential scatters then the electrons in the valence band. After the reemission of the photon, this electron-hole excitation is left behind.

Fig. 11: *Schematic of the RIXS process. From [17]*

also a problem since it is not always obvious, which excitation creates the RIXS signal. Additional interaction such as spin-orbit coupling for magnons are necessary because the photon field excites the electronic system of the sample.

Experimentally RIXS is today a medium resolution technique with a energy resolution $\Delta\hbar\omega \approx$ 0.1 eV. This is due to the fact that the analyzers are not optimized for the final photon energy, which is set by the absorption edge of the element under study. The fourth generation x-ray sources such as energy recovery linac or XFEL provide bright prospects for the evolution of RIXS due to the again dramatically improved source brightness.

5 Conclusion

If one investigates the dynamics of a bulky sample on an atomic scale one has to rely on inelastic scattering methods using neutrons or x-ray photons. Both probes provide specific advantages, which must be weighted before proposing an experiment.

Inelastic neutron scattering provides an energy resolution down to several μeV. If you are interested in life times of the excitations, spin echo methods can even provide higher resolution. The double differential cross section is very well understood for phonon and magnon scattering and hence inelastic scattering may be the ultimate test for models of the dynamic in complex materials. The general problem of inelastic neutron scattering is the limited brightness of todays neutron sources requiring usually several grams of sample to be studied. This limits also the application of complex sample environments such as high pressure cells. Here the new intense spallation source increase significantly the parameter space that can be investigated.

IXS on the other hand is very well suited for the investigation of small sample volumes as the beam already has μm dimensions. As the photon energy is 6 to 8 orders of magnitude larger than the required energy resolution the monochromator development is very demanding as it faces the high energy load of the intense incoming beam. The reciprocal space region that can be probed is basically unlimited, which is very important for high energy excitations or excita-

tions at small momentum transfer e.g. in amorphous materials.

The emerging field of RIXS widens the field of elementary excitations that can be probed to electronic excitations. It can be used to study the coupling between the electrons and the phonon or magnons directly. Being element specific it can be used to distinguish between the ligand or metal dynamics in complex materials and how this affects the functional properties.

Both x-ray and neutron techniques face the challenge that cutting edge instruments are needed to address todays scientific challenges. It is therefore important to understand how these instruments work. Then one may set them up to push the limits further. In combination with the improvement of the sources, which will be provided by the further development of the facilities, novel insight in condensed matter research can be expected.

References

[1] B. Dorner. *Coherent Inelastic Neutron Scattering in Lattice Dynamics*. Springer-Verlag, Berlin, Heidelberg, New York, 1982.

[2] M. J. Cooper and R. Nathans. *Act. Cryst.*, 23:357, 1967.

[3] M. Popovici. *Act. cryst. A*, 31(JUL1):507 – 513, 1975.

[4] K. Lefmann, Ch. Niedermayer, A.B. Abrahamsen, C.R.H. Bahl, N.B. Christensen, H.S. Jacobsen, T.L. Larsen, P. Häfliger, U. Filges, and H.M. Rønnow. *Physica B: Condensed Matter*, 385-386, Part 2(0):1083 – 1085, 2006.

[5] M. Kempa, B. Janousova, J. Saroun, P. Flores, M. Boehm, F. Demmel, and J. Kulda. *Physica B: Condensed Matter*, 385-386, Part 2(0):1080 – 1082, 2006.

[6] A. Hiess, M. Jiménez-Ruiz, P. Courtois, R. Currat, J. Kulda, and F.J. Bermejo. *Physica B: Condensed Matter*, 385-386, Part 2(0):1077 – 1079, 2006.

[7] Wolfgang Schmidt and Michael Ohl. *Physica B: Condensed Matter*, 385-386, Part 2(0):1073 – 1076, 2006.

[8] J. Serrano, A. Bosak, M. Krisch, F. J. Manjón, A. H. Romero, N. Garro, X. Wang, A. Yoshikawa, and M. Kuball. *Physical Review Letters*, 106(20):205501, May 2011.

[9] J. Maultzsch, S. Reich, C. Thomsen, H. Requardt, and P. Ordejon. *Physical Review Letters*, 92(7):075501, 2004.

[10] T. S. Toellner, A. Alatas, and A. H. Said. *Journal of Synchrotron Radiation*, 18(4):605–611, May 2011.

[11] M RENNINGER. doppelspektrometer-auflosungsvermogens. *Zeitschrift Fur Naturforschung Part A-Astrophysik Physik Und Physikalische Chemie*, A 16(10):1110–&, 1961.

[12] Léon Van Hove. *Phys. Rev.*, 95(1):249–262, Jul 1954.

[13] Gen Shirane, Stephen M. Shapiro, and John M. Tranquada. *Neutron scattering with a triple axis spectrometer*. Cambridge University Press, Cambridge, 2002.

[14] G. l. Squires. *Introduction to the theory of thermal neutron scattering*. Cambridge university press, Cambridge, 1978.

[15] S. P. Bayrakci, T. Keller, K. Habicht, and B. Keimer. *Science*, 312(5782):1926–1929, 2006.

[16] T. Keller, P. Aynajian, K. Habicht, L. Boeri, S. K. Bose, and B. Keimer. *Physical Review Letters*, 96(22):225501, 2006.

[17] Luuk J. P. Ament, Michel van Veenendaal, Thomas P. Devereaux, John P. Hill, and Jeroen van den Brink. *Reviews of Modern Physics*, 83(2):705–767, June 2011.

[18] L. Braicovich, M. Moretti Sala, L. J. P. Ament, V. Bisogni, M. Minola, G. Balestrino, D. Di Castro, G. M. De Luca, M. Salluzzo, G. Ghiringhelli, and J. van den Brink. *Physical Review B*, 81(17):174533, May 2010.